

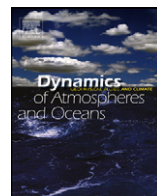


ELSEVIER

Contents lists available at SciVerse ScienceDirect

Dynamics of Atmospheres and Oceans

journal homepage: www.elsevier.com/locate/dynatmoce



Seasonal thermal structure and exchange in Baker Channel, Chile

Christopher M. Aiken^{a,b,*}

^a Estación Costera de Investigaciones Marinas, Pontificia Universidad Católica de Chile, Las Cruces, Chile

^b Centro de Investigación en Ecosistemas de la Patagonia, Coyhaique, Chile

ARTICLE INFO

Article history:

Received 10 October 2011

Received in revised form 31 May 2012

Accepted 12 July 2012

Available online 21 July 2012

Keywords:

Fjord dynamics

Renewal

River plumes

Mathematical models

Chile

Baker Channel

48°S 74°W

ABSTRACT

A series of four field campaigns undertaken between November 2007 and August 2008 in the Baker Channel fjord complex in southern Chile provide a unique record of the seasonal evolution of its vertical and axial structure. The observations document the warming of subsurface waters during the summer and autumn of 2008 creating a subsurface temperature maximum that persists at the channel head until the following spring. An analysis of the observed horizontal and vertical structure is used to infer that the subsurface heating owes to the seasonal intrusion of relatively warm water from Penas Gulf. A series of numerical simulations provide support for the hypothesis that seasonal density fluctuations in the Penas Gulf are responsible for modulating the exchange of intermediary waters and maintaining anomalously warm water at the channel head from autumn until the following spring. The exchange mechanism involves adjustment of the Baker Channel density field to the summer buoyancy increase in the Penas Gulf, which creates an inflow of relatively warm water that fills the channel below the level of the brackish seaward flowing surface layer. The predominantly seasonal renewal of intermediary waters in Baker Channel contrasts with the more usually synoptic nature of above sill exchange in fjords.

© 2012 Elsevier B.V. All rights reserved.

1. Introduction

While a concerted research effort over recent decades has provided an overview of the water properties and general circulation patterns in Chile's extensive fjords region (e.g. Pickard, 1971; Sievers

* Correspondence address: Estación Costera de Investigaciones Marinas, Osvaldo Marín 1672, Las Cruces, Chile.
E-mail address: chris@foca.cl

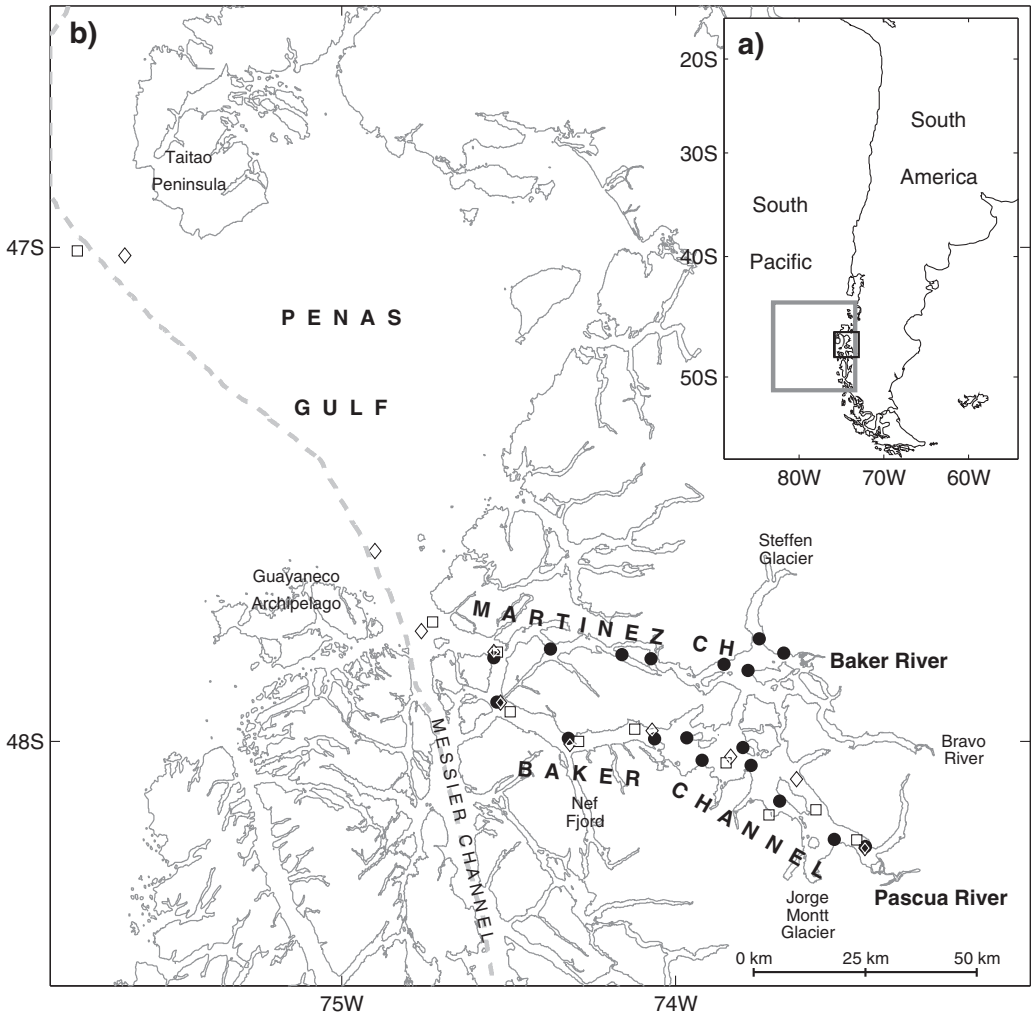


Fig. 1. (a) Geographical location of the study area, showing the domains of the outer and inner nested models. (b) Map of the BPE and Penas Gulf. The locations of observations from the Hudson, Cimar Fiordo 2, and LOBO campaigns are marked by the squares, diamonds and closed circles, respectively. The dashed line marks the route corresponding to the thermosalinograph data shown in Fig. 4.

and Prado, 1994; Silva et al., 1995, 1998; Sievers et al., 2001; Silva and Guzmán, 2006), the variability in the system, and the mechanisms responsible for this, remain largely unaddressed. In the following the mechanism driving exchange in the estuary of the Baker and Pascua rivers, a zonally oriented complex of channels and fjords that separates the northern and southern Patagonian ice-fields at approximately 48°S (Fig. 1), is investigated. This system – referred to here as the Baker–Pascua Estuary (hereafter BPE) and whose principal branch is the Baker Channel – receives an annual mean freshwater flux of over $1600 \text{ m}^3 \text{ s}^{-1}$ from the Baker and Pascua rivers, plus contributions from the Jorge Montt glacier and the Bravo and Steffen rivers (Fig. 2). The BPE is likely to be subject to significantly altered forcing conditions over coming decades, as reduced precipitation and accelerated ice-sheet melt back associated to climate change (Fuenzalida et al., 2007), plus possible hydroelectric dam construction on the Pascua and Baker rivers, may significantly alter the river discharge regime into the system. This has intensified interest in the area and hastened efforts to study and understand the system.

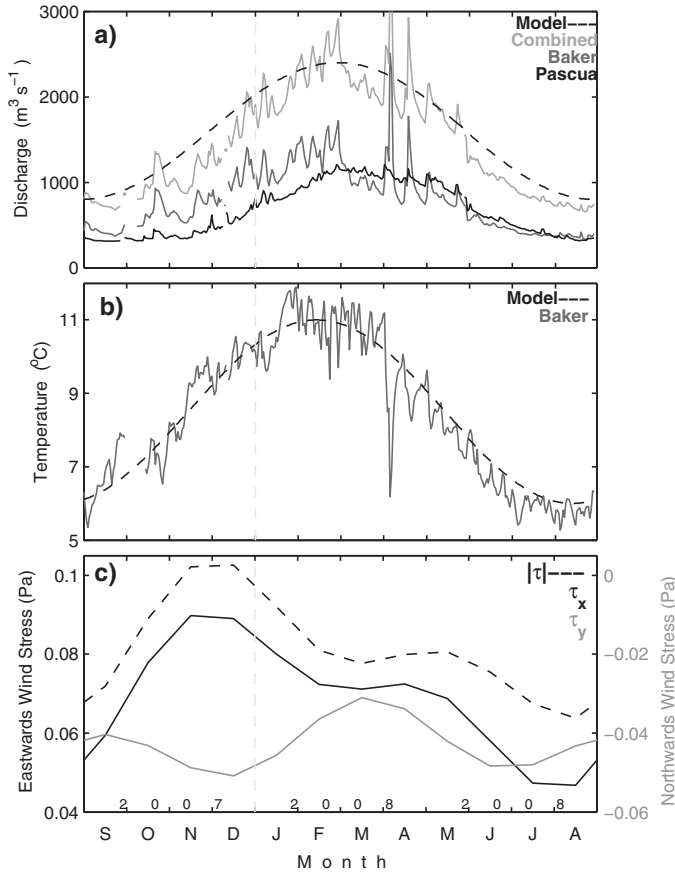
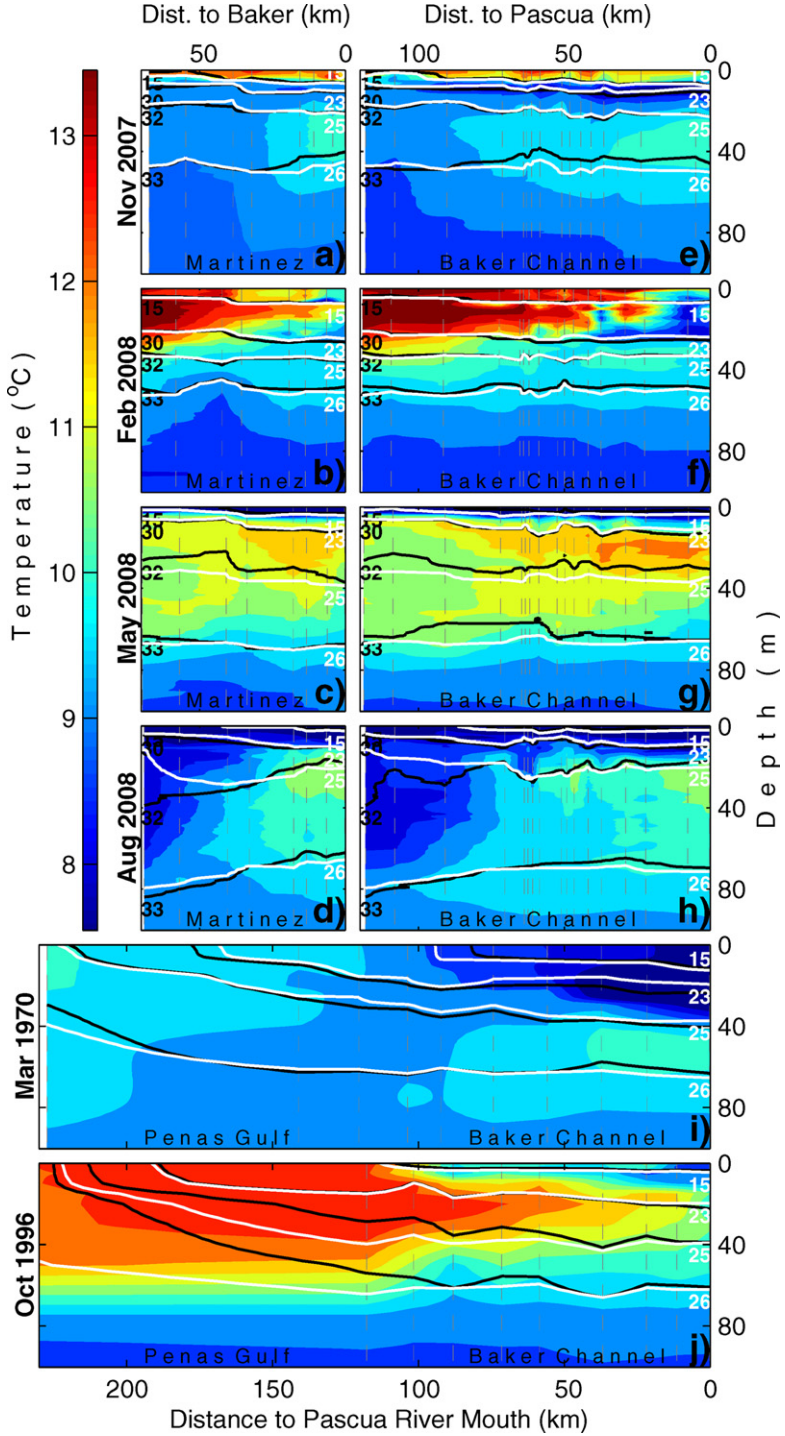


Fig. 2. (a) Observed daily mean river discharge from the Baker (dark) and Pascua (medium) rivers. The combined (light) and idealised seasonal cycle of river discharge used in the model (dashed) are also indicated. (b) Observed daily mean temperature of Baker river (solid) and the idealised seasonal cycle used in model (dashed). (c) Monthly mean wind stress in Penas Gulf from Quikscat. The dramatic increase in discharge of the Baker and decrease in its temperature on April 6, 2008 corresponds to the sudden drainage of the ice-dammed lake Cachet 2.

While the peak in riverine freshwater flux into the BPE occurs during late summer together with the glacial melt maximum, the total river discharge remains above $700 \text{ m}^3 \text{ s}^{-1}$ on average throughout the year (Fig. 2). As a result, a brackish surface layer is a permanent feature throughout the BPE. Although typically less than 10 km wide, the BPE reaches depths in excess of 1000 m, and the series of internal sills are in general deeper than 200 m. Thus it is the 100 m deep Penas Gulf, the relatively broad shallow bay open to the west into which the BPE empties, that limits exchange with the ocean. While the Penas Gulf is sufficiently deep that exchange will not be hydraulically controlled (Farmer and Freeland, 1983), it will be shown that heat and salt fluxes in the Penas Gulf may control the subhalocline thermal structure within the BPE. Shelf conditions off-shore of the Penas Gulf are likely to be influenced by the Cape Horn Current, the eastern boundary current of the South Pacific. Knowledge of this feature and its exact role in coastal processes, however, is severely limited by a paucity of observations (Silva and Neshyba, 1977).

The historical record of observations taken of the BPE water column is limited to those gained during the Hudson 70 (Pickard, 1971) and Cimar-Fiordo 2 (Rojas et al., 2002) expeditions, performed in March 1970 and October 1996, respectively. Temperature transects along the axis of the Baker Channel from the two expeditions are shown in Fig. 3. In both cases a subsurface temperature maximum was



observed within the BPE, but while the Hudson 70 summer cruise uncovered a general trend for temperature to decrease with proximity to the channel head throughout the water column (Fig. 3j), in the Cimar-Fiordo 2 spring cruise (Fig. 3i) the temperature maximum was found only at the head of the channel (Sievers et al., 2001). The relatively large differences in the observed thermal structure between the two campaigns implies a substantial level of natural variability, however, clearly neither the time scales involved nor the mechanism responsible can be determined.

In general, fjords are examples of deep, highly stratified estuaries. In classical estuarine circulation, a subsurface return flow is required to balance entrainment into the seaward flowing surface advected river plume. In fjords, however, the brackish surface layer commonly occupies only a small fraction of the water column, and the circulation of deeper waters may be relatively decoupled from river discharge, depending more strongly on the density structure external to the fjord. While exchange between the ocean and deep fjord waters is constrained below the level of the shallowest sill, the “intermediary waters” found between the halocline and sill height can adjust to baroclinic forcing on the adjacent shelf. In fact, in many fjords external pycnocline fluctuations have been found to be the principal driver of exchange between the fjord and shelf in the intermediary layer (Stigebrandt, 1990). The pycnocline excursions are commonly synoptic in nature and associated with wind-driven upwelling (e.g. Svendsen, 1980; Arneborg, 2004; Cottier et al., 2007) or variations in the strength of adjacent geostrophic currents (Klinck et al., 1981; Janzen et al., 2005). As a result, when vertical heat and salt fluxes within the fjord are weak then the volume fluxes into the fjord and the rate of intermediary water renewal can be estimated from the internal pycnocline excursions (Aure et al., 1996; Arneborg, 2004).

Being located below the brackish surface estuarine layer and above the level of the Penas Gulf sill, the previously observed subsurface temperature maxima correspond to features of the intermediary circulation. Although such temperature profiles, of type 4 in the Pickard and Stanton (1980) classification, are relatively rare in other fjord regions, similar subsurface temperature maxima intensified towards the estuary head, and occasionally found at multiple depths, have been observed in various other near-by Chilean fjords, suggestive of a possible common cause (Pickard, 1971; Silva and Calvete, 2002). Nonetheless, while a number of possible explanations have been ventured (Pickard, 1971; Silva and Calvete, 2002) this phenomenon and its significance for exchange have not received further attention. The absence of any plausible localised heat source to explain the channel head subsurface temperature maximum observed in Cimar-Fiordo 2 implies the existence of episodic heating events combined with a gradual subsurface cooling that increases towards the channel mouth. In the following the mechanism producing the subsurface heating within the BPE is investigated.

In order to address this issue, a series of four field campaigns were undertaken between November 2007 and August 2008 to observe the evolution of the water column along its length and throughout the year. These observations, together with a series of numerical simulations, indicate that horizontal exchange driven by the seasonal cycle of off-shore heat and salt fluxes alone may be sufficient to explain the thermal structure observed at the estuary head, without the necessity of direct heating at the fjord head or synoptic-scale events to initiate or control flushing.

The observational data acquired during the new campaigns is presented in Section 2 and compared to the historical data. In Section 3 the observations are analysed to demonstrate that the observed heating is likely to result from advection of waters from Penas Gulf. This result is supported by numerical simulations that are presented in Section 4, and conclusions are made in Section 5.

2. Observations

Field campaigns were carried out in November 2007 and February, May and August 2008, corresponding to late spring, late summer, late autumn and late winter, respectively. Each campaign

Fig. 3. Transects along the Martínez (a–d) and Baker (e–h) channels of the temperature (shaded), density (white contours) and salinity (black contours) observed during the field campaigns. Similar transects along Baker Channel and through Penas Gulf from the Hudson and Cimar Fiordo 2 cruises are shown in (i) and (j), respectively. The locations of observations are marked by dashed lines, and the geographical location of the stations are indicated in Fig. 1b.

involved the measurement of temperature and salinity profiles down to 100 m depth from a series of stations spread along the length of the BPE, between the mouth of the Pascua River and Porcia Island at the entrance to Baker Sound (Fig. 1b), covering a distance of approximately 100 km. The observations were all taken above the level of the Penas Gulf sill and hence correspond to estuarine and intermediary waters. The instruments used were a Seabird Electronics SBE25 CTD for the first campaign and an Idronaut OceanSeven 304 CTD for the remaining campaigns. In all campaigns the CTD casts were performed from the 14 m wood-hulled vessel *Santa Fe*.

In addition to the discrete vertical casts, continuous underway surface observations were obtained from a thermosalinograph (TSG) installed on board the *M/N Evangelistas* as part of the FOCA (*Ferries Observando los Canales Australes*) project (Aiken et al., 2011). The *Evangelistas* traversed the Penas Gulf twice per week over the period October 2007 to March 2008, yielding a record of surface temperature and salinity that coincides with the first two of the field campaigns. The ship's route is indicated in Fig. 1b and the data from the vicinity of Penas Gulf are presented in Fig. 4.

Fig. 3 shows transects of the observed temperature, salinity and density in each campaign along the Martínez and Baker Channels, the main northern and southern branches of the BPE, respectively. It may be appreciated that isohalines generally run parallel to isopycnals, indicating that density is dominated by salinity and hence that temperature may be considered to first order a passive tracer within much of the fjord. The fact that density is dominated by salinity is demonstrated in Fig. 4. The right hand column plots

$$\Phi = \arctan \left(\frac{\rho_T |\Delta T|}{\rho_S |\Delta S|} \right) - \frac{\pi}{4}, \quad (1)$$

where ρ is the density, T the temperature, S the salinity, the difference Δ is taken over consecutive campaigns, and subscripts denote partial derivatives with respect to the indicated variable.

Φ may be recognised as the Turner angle – the arctangent of the density ratio – offset so as to fall on the interval $(-\pi/4, \pi/4)$. Values of $\Phi > 0$ ($\Phi < 0$) indicate that density changes between consecutive campaigns are driven by temperature (salinity). Clearly density in the BPE is predominantly driven by salinity, especially towards the estuary head. In general, temperature only dominates when the density differences (third column of Fig. 4) are weak. As a result, temperature may be considered to first order as a passive tracer, and its evolution can serve to diagnose the timing of, and mechanisms responsible for, exchange of intermediary waters.

To aid the following discussion a number of water masses within the BPE are defined following Guzmán and Silva (2002): river water (RW, $\sigma_t < 15 \text{ kg m}^{-3}$ or $S < 15 \text{ psu}$), Estuarine water (EW, $15 < \sigma_t < 23 \text{ kg m}^{-3}$ or $10 < S < 30 \text{ psu}$), Modified Subantarctic water (MSAW, $23 < \sigma_t < 26 \text{ kg m}^{-3}$ or $30 < S < 33 \text{ psu}$), and Subantarctic water (SAW, $26 < \sigma_t \text{ kg m}^{-3}$ or $33 < S \text{ psu}$). The density and salinity boundaries between the water masses are equivalent for most of the BPE due to the latter's dominance of the former. The evolution of each of these water mass layers over the course of the four campaigns is summarised below.

2.1. River water

The RW layer corresponds to the relatively fresh or brackish water generally found above a sharp halocline, here denoted nominally by the 15 psu isohaline. Typical of high run-off fjords, the RW layer tended to be well-mixed, with only slight variations in temperature and salinity between the surface and top of the halocline Pickard and Stanton (1980). The thickness and extent of the RW layer was strongly linked to the river run-off seasonal cycle (Fig. 2), consistent with the fact that the degree of turbulent mixing depends upon the river discharge. During the summer peak flow conditions observed in the February campaign, RW covered the upper 4–7 m of the BPE, thinning with distance downstream. The 2 psu isohaline outcropped over 70 km downstream from the Pascua river mouth and was located at 6 m depth at the Baker river mouth (Fig. 5a).

The RW layer was thinnest during the May (autumn) and August (winter) campaigns, consistent with the reduction in river discharge. Nonetheless, even in winter RW covered the inner 50 km of the BPE, and the halocline salinity gradient exceeded 2 psu m^{-1} throughout the BPE, demonstrating a permanent strong stratification. In the November (spring) campaign the RW layer was similarly deep

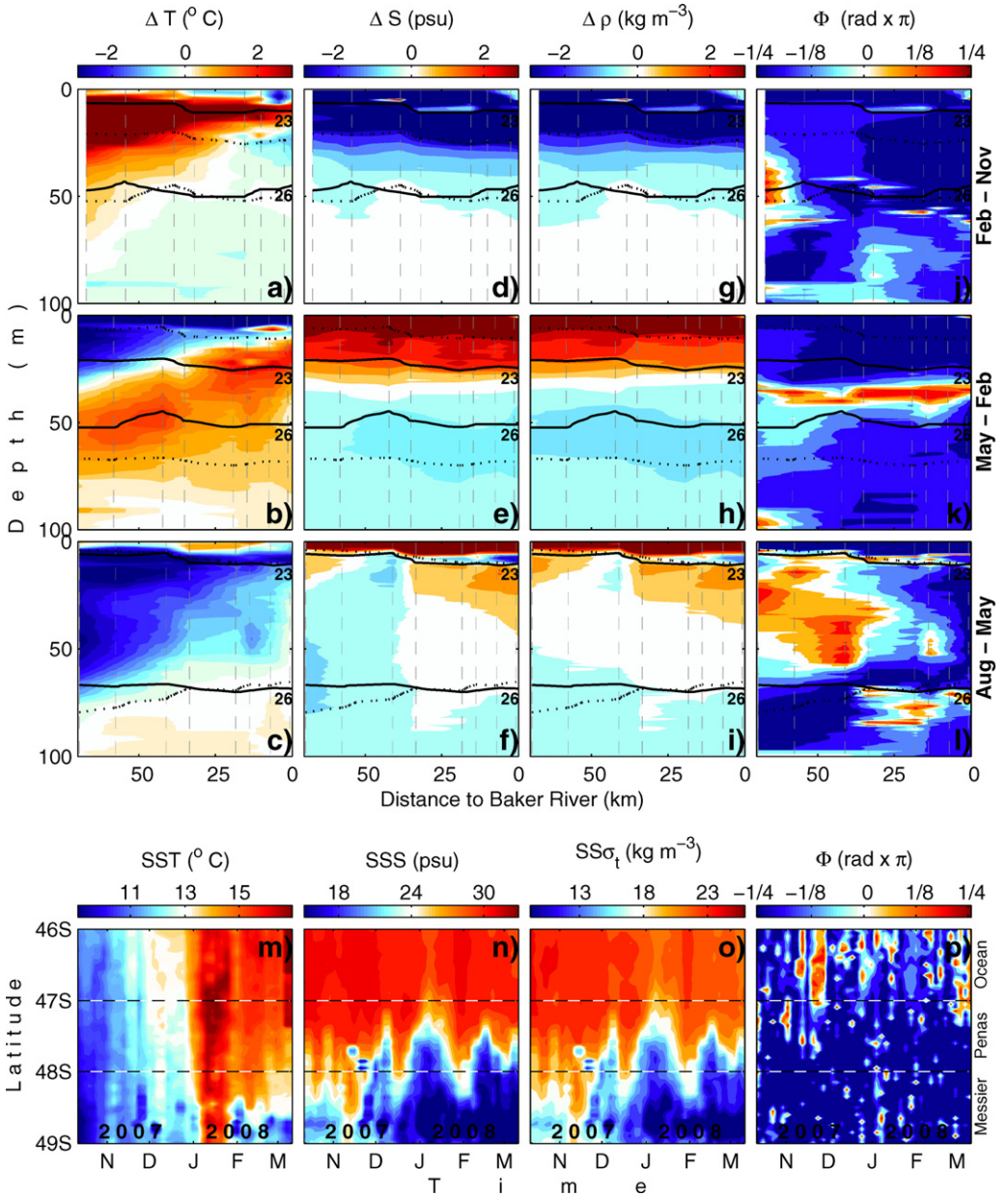


Fig. 4. Change in the temperature (a–c), salinity (d–f) and density (g–i) within Martínez Channel between consecutive campaigns. The relative contributions of temperature and salinity to the change in density is indicated by the value of the Turner angle Φ (j–l). The original (final) positions of the 1023 and 1026 kg m^{-3} isopycnals over each interval are indicated by the solid (dashed) contours. The sea surface temperature (m), salinity (n), density (o) and Φ (p) within Penas Gulf as observed from a thermosalinograph installed on the *M/N Evangelistas*. The ship repeated the route, shown in Fig. 1, twice per week.

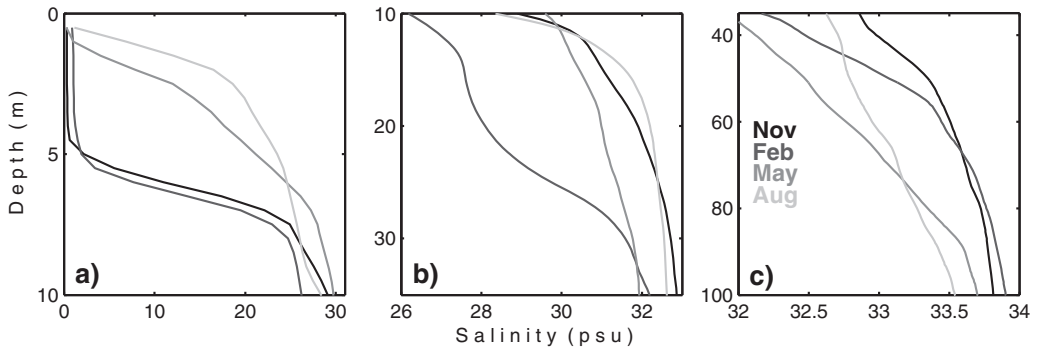


Fig. 5. The vertical salinity profile at the Pascua river mouth for each of the four campaigns. Note that the scale of both x and y axes changes between each panel.

and fresh at the river mouths as in summer, but thinned more rapidly with distance. The temperature of the RW followed closely the seasonal cycle of atmospheric temperature, varying from above 13 °C in summer to below 5 °C in winter.

2.2. Estuarine water

In spring the thin EW layer was largely composed of “winter water” (WW) – cool EW formed at the channel head during the previous winter’s low-flow conditions that is subsequently covered by warmer spring RW. The winter cooling of subhalocline waters responsible for WW production may be appreciated in Fig. 4c. The lens of WW was located at the base of the halocline, laying between relatively warm MSAW and RW. The EW layer was observed to experience largest changes during the summer. Summer EW temperature was up to 4 °C greater than in spring (Fig. 4a), and in fact exceeded that of RW at most locations along the length of the BPE. Although Fig. 4a demonstrates a clear trend for the summer EW heating to decrease with distance from the ocean, this was not evenly distributed in the horizontal nor vertical, and remnants of WW remained at some locations and depths, in particular at the base of the halocline, producing multiple small temperature inversions between Nef fjord and the river mouths (Fig. 3b and f). Between November and February the base of the layer descended from 7 m to 25 m depth along the length of the BPE, associated with a large decrease in salinity in the upper 30 m (Fig. 5). Despite the substantial summer heating of EW, the density decrease of waters above 25 m was due almost entirely to freshening (Figs. 4g and j and 5). By May (autumn) the 1023 kg m⁻³ isopycnal (30 psu isohaline) had returned almost to its pre-summer position and had shoaled slightly more by August (winter). The corresponding buoyancy loss above 25 m was again due to salinity changes (Fig. 4h and k). As will be discussed in the following, the thickening of the EW layer and the pattern of warming are highly suggestive of up-channel transport and interleaving in the EW layer over summer.

2.3. Modified Subantarctic water

Throughout the Chilean fjords region MSAW has been identified to form along the shelf through vigorous mixing of SAW with EW (Guzmán and Silva, 2002). Two distinct branches of MSAW may be appreciated within the BPE, separated by the 32 psu isohaline, and referred to here as upper and lower MSAW. In November 2007 (Fig. 3a and e) a pronounced temperature maximum was observed within the lower MSAW layer (i.e. between isohalines 32 and 33 psu). The feature was present along much of the length of the BPE, but intensified towards the mouths of the Baker and Pascua rivers. By February the MSAW layer had thinned to ≈25 m from its spring value of ≈40 m, associated to the thickening of the EW layer without a corresponding deepening of the 1026 kg m⁻³ isopycnal. Over the summer

MSAW warmed moderately towards the channel mouth, but cooled slightly towards the head of the estuary (Fig. 4a).

The May 2008 expedition encountered a significantly warmer and thicker MSAW layer compared to that seen in the summer, in particular the upper layer. Between February and May the 1023 kg m^{-3} isopycnal shoaled by up to 20 m, the 1026 kg m^{-3} isopycnal deepened by close to 20 m, and the temperature at the head of the channel within the upper MSAW layer increased by over 3°C . Fig. 4 reveals that during autumn the water column freshened quite uniformly by ≈ 1 psu below 30 m depth, and increased substantially in salinity above this level. The band of positive Φ visible in Fig. 4k reflects the fact that salinity did not change at this depth, and hence that the small changes in density were due to heating. By August 2008, the upper MSAW layer was observed to have thinned and cooled while the lower MSAW layer continued to thicken and homogenize vertically (Fig. 3d and h). The winter cooling at the mouth of the BPE had a greater effect upon the density than the slight freshening in the same region.

2.4. Subantarctic water

Temperature variations within the fraction of the SAW layer that was observed changed relatively little over the course of the campaigns, in particular towards the head of the BPE. Temperature was horizontally uniform in summer and autumn, and had a slight up-channel gradient in spring and winter due to cooling at the channel mouth.

2.5. Historical observations

The thermohaline structure documented above strongly resembles that observed in the two previous field campaigns to the BPE region. In the spring of 1996 the MSAW layer presented a channel temperature maximum lying below a lens of WW that was of similar intensity to, although located ≈ 10 m deeper than, that found in November 2007. The cool WW layer is steadily eroded during the spring and summer, so the fact that this layer was deeper, thicker and slightly cooler in October 1996 than in November 2007 is consistent with the slightly earlier time of year at which the observations were taken. Similar down-channel temperature gradients in EW and MSAW were present in both March 1970 and February 2008. Given the trend for thickening of the MSAW layer during late summer, the differences in MSAW layer thickness are consistent with the fact that the Hudson observations correspond to a slightly later stage in the year.

The fact that the thermohaline structures observed in spring 2007 and summer 2008 were qualitatively consistent with those recorded previously in the same seasons is strongly suggestive that the recurring features correspond to the seasonal cycle and are not an artifact of aliasing of sub-seasonal variability. If non-seasonal processes dominated the evolution of the thermal structure in the BPE it would be unlikely to observe the recurrence of these strong features in the same season of different years. In addition, the inferred retention of a body of warm MSAW at the channel head from autumn until the following spring provides compelling evidence that subseasonal variability within the upper reaches of the BPE must be weak. The possibility for seasonal forcing alone to generate the observed subsurface heating supported by the numerical modelling presented below.

3. Source of subsurface heating – vertical or horizontal?

The observations reveal two distinct heating events of subsurface waters at the head of the BPE – EW in summer and MSAW in autumn. In this section we discuss whether these heating events are likely to owe to vertical or horizontal heat fluxes.

3.1. Summer EW heating

A possible source of the summer heating of EW is a net downwards heat flux from the relatively warm surface river water. Although the sharp pycnocline would tend to inhibit vertical mechanical mixing, over longer time-scales a net vertical heat flux may still occur, albeit more slowly, through

molecular diffusion. Given the greater molecular diffusion rate for temperature than for salt, a subsurface warming could occur without a corresponding salinity decrease, a process known as double diffusion (Padman and Dillon, 1987). Inspection of the distribution and timing of the heating observed, however, allows the hypothesis of it having a vertical diffusive origin to be rejected. A vertical flux of heat from the warm surface river water, be it mechanically or molecularly driven, would have to erode completely the cold WW lens at the estuary head before producing a warming at greater depth. However, the subsurface heating of EW in the BPE commenced in February even while pockets of cool WW persisted above at the base of the halocline. This is particularly apparent at the mouth of the Baker River in Fig. 3b, where the EW is significantly warmer than both the WW and RW lying above it. In fact, the fact that WW persisted through to summer in itself implies that the subhalocline vertical diffusion of heat is weak. Weak vertical diffusion is not surprising given the very strong pycnocline present in the upper reaches of the BPE throughout the year – the maximum vertical density gradient at the Pascua river mouth exceeded 15 kg m^{-4} (a local buoyancy frequency $N \approx 0.38 \text{ s}^{-1}$) in November and February, and even during winter low flow conditions exceeded 6 kg m^{-4} ($N \approx 0.24 \text{ s}^{-1}$). Extremely weak or nonexistent vertical mixing has been reported for buoyant surface layers that are much more weakly stratified than the BPE (Fer, 2009).

The possibility of direct solar heating of the subsurface waters is unlikely due to the high albedo of the rock-flour laden river water, and the fact that the heating lags the seasonal cycle of solar radiation. As a result, there is little evidence to support a significant downwelling heat flux into the EW layer, and hence the heating must involve horizontal advection of warm waters from outside the BPE.

The observed EW warming in summer is consistent with an intrusion of warm surface Penas Gulf water below the RW layer. The persistence of remnants of WW within the EW layer during the summer heating (Fig. 3b and f) is highly suggestive of interleaving of the warm external waters as they penetrate into the Baker and Martínez channels at their equilibrium density. It is possible that the February campaign may have coincided with the EW exchange event, and as such it is likely that the intrusion of warm water continued up to the estuary head. Horizontal advection of external waters into the BPE would require a reorganisation of the internal density field to accommodate the mass flux, and this was indeed seen. The 1023 kg m^{-3} isopycnal deepened by 18 m over the summer which, in the absence of significant internal mixing, implies the import of $\approx 2 \times 10^{10} \text{ m}^3$ of warm EW from outside the BPE, or an average volume flux of $\approx 3000 \text{ m}^3 \text{ s}^{-1}$ over the course of the summer. This corresponds to a mean up-estuary velocity averaged over the width of the BPE and depth of the EW layer of $\approx 2.5 \text{ cm s}^{-1}$.

If the subhalocline water properties are indeed weakly modified within the BPE due to the relatively weak vertical diffusion, then the source of the warm summer EW may be inferred by tracing isopycnals to the location where they outcrop. In the summer campaign the 15 psu isohaline marking the upper edge of the EW layer did not intersect the surface within the BPE, while in the Hudson campaign and in the FOCA thermosalinograph record, the 1023 and 1026 kg m^{-3} isopycnals (15 and 30 psu isohalines) were observed to outcrop within the Penas Gulf. Although no concurrent observations of the Penas Gulf water column are available, wind driven mixing of the warm brackish surface waters observed in the Penas Gulf during summer (Fig. 4m and n) could be expected to depress the 1023 kg m^{-3} isopycnal, and hence drive adjustment within the BPE. The values of Φ shown in Fig. 4p suggest that freshening contributes substantially more to the buoyancy increase of near surface waters in Penas Gulf than warming.

3.2. Autumn MSAW heating

As was seen for summer EW heating, the autumn heating of MSAW at the channel head is consistent with horizontal advection of external waters. The observed thickening of the MSAW layer by 40 m over autumn requires a mean up-estuary volume flux of $\approx 12,000 \text{ m}^3 \text{ s}^{-1}$ from the Penas Gulf, implying an average up-estuary velocity of $\approx 3.5 \text{ cm s}^{-1}$. Again it is plausible that adjustment to external isopycnal deepening in Penas Gulf could have resulted in the transport of warm MSAW into the BPE. This would also imply an export of EW to explain the shoaling of the 30 psu isohaline, requiring a similar shoaling of this isohaline in Penas Gulf. The modelling presented below supports this hypothesis.

While horizontal advection can explain the MSAW heating, there also exists evidence to support the alternative hypothesis involving a net downward heat flux due to mixing of the overlying warm

EW water during autumn. The relatively strong subhalocline vertical salinity gradient present in summer weakened substantially over the autumn and winter, as waters above 30 m became saltier and those below freshened (Fig. 5). This is consistent with vertical mixing and implies a vertical diffusion coefficient for salinity $K_S \approx 0.7 \text{ cm}^2 \text{ s}^{-1}$ that is not implausible. This value is determined from $K_S = F/S_z$, where F is the upwelling salt flux across 30 m at the channel head averaged over 3 months, S_z is the vertical salinity gradient at the channel head in summer, and it is assumed that changes in the salinity of MSAW during autumn were solely due to vertical salt fluxes. The observed autumn thinning of the EW layer through erosion at its base is consistent with this scenario.

The degree of heating seen in the MSAW layer (Fig. 4b), however, tends to suggest that a vertical mixing source of heating is unlikely. A measure of the heat content at the head of the BPE integrated over the EW and MSAW layers may be defined as

$$Q = N^{-1} \sum_{x=1}^N \int_{80}^{10} \rho C_p T(x, z) dz \quad (2)$$

where the summation is over the $N=5$ stations closest to the Pascua river mouth, the integral is over the range of depths z from 10 m to 80 m that includes the EW and MSAW layers, C_p is the heat capacity of sea water and ρ is the density. From late February to late May Q increased by $\approx 18\%$, suggesting that the subhalocline waters at the head of the BPE gained heat during the autumn. Although surface heat fluxes were inferred to play no role below the pycnocline, clearly the possibility exists that the EW layer could have continued to heat during the autumn via the process outline above. However, if it is assumed that the summer up-channel advection of warm external EW continued until the temperature of EW at the BPE head equalled that at the mouth, the inferred autumn increase in the combined heat content is still $\approx 5\%$. The fact that the subpycnocline water column heat content is estimated to have increased during the autumn implies that the water column heating observed in May is unlikely to be due to vertical diffusion of heat from the overlying EW. As a result, and as was deduced for the summer heating of EW, a net horizontal heat flux is the most likely explanation for the observed autumn heating of MSAW at the channel head.

4. Numerical simulation of circulation in the BPE

4.1. Model configuration

In order to investigate the mechanisms responsible for the inferred exchange in the BPE, a series of numerical simulations of the circulation within the BPE and adjacent shelf were performed using the Regional Ocean Modelling System (ROMS), a widely used free-surface, hydrostatic, primitive equation ocean model (Shchepetkin and McWilliams, 2005). Previous work has confirmed the utility of ROMS for studies of estuarine and shelf circulation (e.g. MacCready and Geyer, 2001; Warner et al., 2005; Hetland, 2005).

The numerical simulations involved running two nested models – an outer model covering the section of coast adjacent to the Penas Gulf, and an inner model that provided greater resolution of the Penas Gulf and entrance to the BPE. A nested model configuration was chosen to allow both shelf and fjord processes to be included, as well as to improve the quality of the open boundary conditions provided to the inner model. The outer domain covered the region bounded by 74°W , 82°W , 52°S and 44°S , approximately 650 km in each direction, while the inner domain covered only the Penas Gulf and BPE (Fig. 1). Grid dimensions of 128×128 in both cases gave uniform horizontal resolutions of approximately 5 km and 2 km. In the vertical, 30 stretched terrain-following levels were used in each case, concentrated towards the surface using the s -level stretching parameters $\theta_s = 5$, $\theta_b = 0$, and $h_c = 20$ (Song and Haidvogel, 1994). Bathymetry was derived from ETOPO2 (U.S. Department of Commerce, 2006) merged with sounding data from the nautical charts 9000 and 9100 of the Chilean Navy Hydrographic and Oceanographic Service (SHOA). The common bathymetry was smoothed following standard practice to reduce the generation of spurious currents associated with the hydrostatic inconsistency (Mellor et al., 1994). Given the complexity and very small spatial scales involved, it was

chosen to represent the BPE as a single 100 km long, 10 km wide zonal channel with a constant depth of 300 m in both domains.

Despite this idealisation, the model was able to reproduce the observed vertical structure at the channel head to a reasonable degree, suggesting that the exact detail of the BPE's complex geometry may be of secondary importance to subhalocline exchange processes. This may be due to the relative unimportance of frictional effects.

River input was applied at the head of the idealised BPE as a point source of momentum, temperature and salinity. The annual cycle of combined discharge and water temperature from the Baker and Pascua rivers was estimated from daily flow data recorded automatically by the Chilean *Dirección General de Aguas* from March 2003 to the present (Fig. 2). The mass flux was applied evenly across the width of the channel and varied with depth z as $\cos((\pi/2)(z/10))$ down to 10 m depth. Wind forcing was provided by a monthly climatology calculated from 9 years of Quikscat winds from 2000 to 2008, with winds inside the BPE set equal to that at the nearest resolved location within Penas Gulf. Climatologies of heat flux, momentum, temperature, salinity and sea surface elevation for determining initial and boundary conditions in the outer model were calculated from the ECCO (Estimating the Circulation and Climate of the Ocean) data-set, a data-constrained solution of the MitGCM (Wunsch and Heimbach, 2007). The annual cycles of temperature, salinity and momentum applied on the open boundaries of the inner model were determined from the final year of a five year simulation of the outer model. In both models the radiation/nudging conditions of Marchesiello et al. (2001) were employed to temperature, salinity and velocity at the three open boundaries, with nudging time-scales for incoming (outgoing) wave propagation of 1 day (100 days), while a zero gradient condition was applied to open boundary surface elevation. Volume conservation was enforced within the domain via appropriate adjustment of the vertically averaged velocity on the open boundaries. A standard temperature-dependent heat flux correction term determined from bulk formula was used that effectively relaxed sea surface temperature towards climatology in each case. The turbulent closure scheme of Large et al. (1994) was used and the harmonic horizontal viscosity and diffusivity were set to $100 \text{ m}^2 \text{ s}^{-1}$ and zero, respectively.

The outer model was spun-up from rest over 5 years, by which time the simulated circulation had reached a statistically stationary state. The inner model was then initialised from the final state of the outer model and run for a further five years. In the following, the results presented correspond to the fields from the inner model.

4.2. Simulated exchange in the BPE

Seasonal zonal transects taken along the axis of the BPE and through Penas Gulf are shown in Fig. 6a–d. It may be seen that the simulation was able to qualitatively recreate a number of key aspects of the observed thermohaline structure within the BPE (cf Figs. 3 and 6). Driven by weaker (stronger) winds and decreased (increased) river discharge, the thickness of the estuarine circulation layer thinned (thickened) during winter (summer), consistent with the observations. The autumn deepening and spring shoaling of the 1026 kg m^{-3} isopycnal was also well represented in the model. Most notably, the relatively rapid summer/autumn heating of intermediate waters and gradual cooling for the remainder of the year was well represented. Warming of subsurface waters occurred in the model from March until August, and the peak up-channel temperature occurred in May, consistent with the observations. The fact that the temperature structure at the estuary head was well reproduced suggests that the model captures the processes driving subsurface heating. It may be noted, however, that the model does not reproduce the observed winter cooling at the mouth of the BPE. As discussed further below, this may owe to the various simplifications made in the model that are likely to be of increased relevance within the lower reaches of the BPE. Nonetheless, the success of the model in reproducing the channel head temperature evolution suggests that the processes driving cooling at the channel mouth are of secondary importance for the summer/autumn exchange events of primary interest here.

The source of the subsurface warming in the model can be readily determined. In an additional experiment in which the surface heat flux within the BPE was set to zero, the subhalocline thermal structure was almost identical to that in the control simulation, confirming that vertical heat transport from the surface is not responsible for the modelled subsurface warming. The role of horizontal

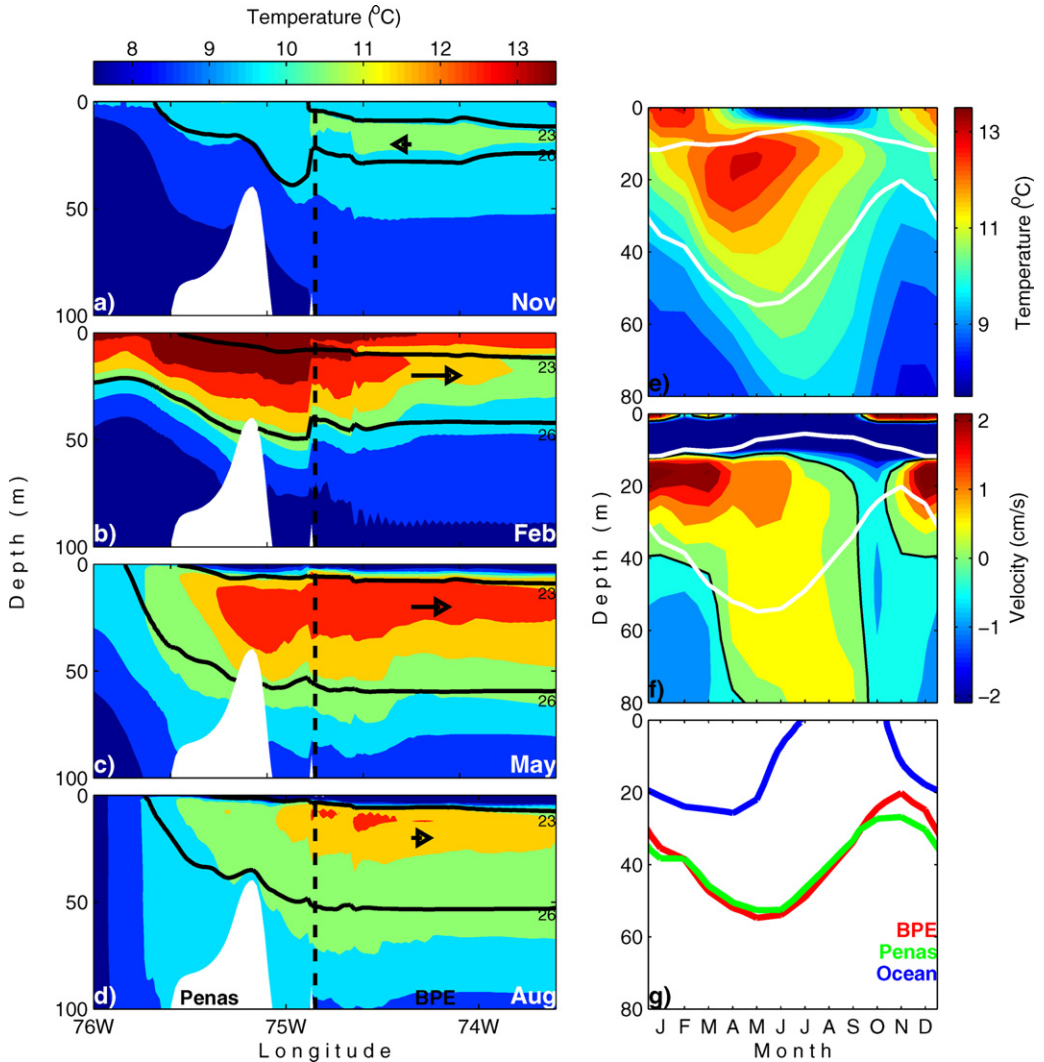


Fig. 6. (a–d) Zonal transects along the axis of the BPE and across the Penas Gulf of the monthly mean temperature (shaded) and density (contours) from the model for the months indicated. Vectors indicate the monthly mean along-channel velocity at 20 m depth from the model. (e) Evolution of the monthly mean temperature profile from the BPE over the course of the year as simulated by the numerical model. (f) As in (a) but for along-channel velocity. Positive velocity signifies transport towards the channel head. (g) Evolution of the depth of the 1026 kg m^{-3} isopycnal from the BPE (red), south east corner of Penas Gulf (green) and western open boundary of the model (blue). For reference the depths of the 1023 and 1026 kg m^{-3} isopycnals in the BPE are marked by white contours in (e) and (f). (For interpretation of the references to color in this figure legend, the reader is referred to the web version of this article.)

advection in the model is demonstrated by the fact that the subsurface heating coincides with the development of eastwards flow below the pycnocline (Fig. 6e and f). A horizontal advective heat transport into the BPE occurs during summer and autumn and is well correlated with the temperature increase and density field adjustment. Strongest inflow below the halocline coincided with the period of fastest shoaling (deepening) of the 1023 (1026) kg m^{-3} isopycnal (Fig. 6e–g). Thus horizontal advection of waters external to the BPE is responsible for the MSAW heating in the model.

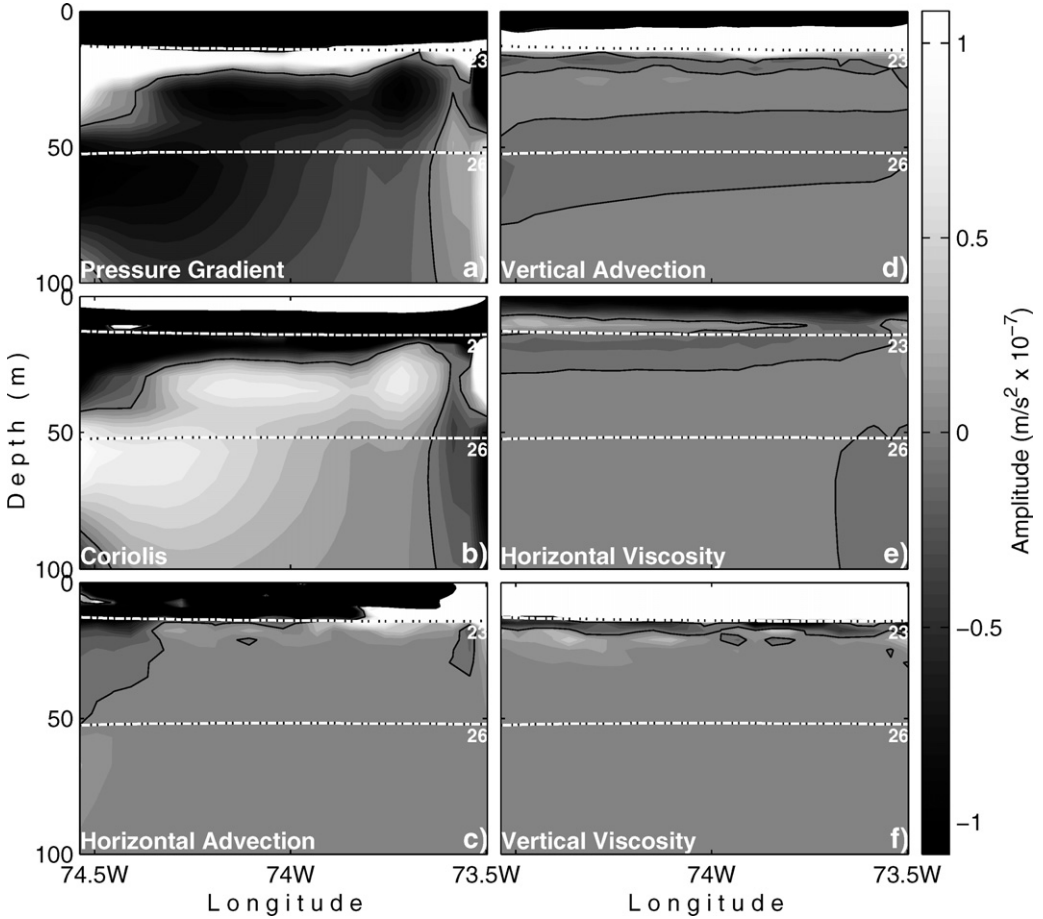


Fig. 7. Mean cross-channel average of each term in the along-channel momentum equation (3) within the uppermost 100 m of the modelled BPE.

Fig. 7 shows the mean value within the BPE of each of the terms in the along-channel momentum balance,

$$\underbrace{u_t}_{\text{Acceleration}} + \underbrace{uu_x + vu_y}_{\text{Horizontal Advection}} + \underbrace{wu_z}_{\text{Vertical Advection}} - \underbrace{fv}_{\text{Coriolis}} = \\
 - \underbrace{\phi_x}_{\text{Pressure Gradient}} + \underbrace{(K_M u_z)}_{\text{Vertical Viscosity}} + \underbrace{D}_{\text{Horizontal Viscosity}},$$

where u , v and w are the eastwards (along-channel), northwards and vertical velocity components, respectively, f is the Coriolis parameter, ϕ is the dynamic pressure, K_M is the vertical eddy viscosity, D represents the horizontal diffusive term, and subscripts denote partial derivatives to the indicated variable. While all terms are dynamically important in the RW layer, below the halocline the pressure gradient and Coriolis terms are at least an order of magnitude larger than all other terms. This indicates that the subpycnocline circulation in the BPE is dominantly geostrophic, and hence that horizontal motion is balanced by fluctuations in the local density field. The cross-channel momentum balance (not shown) confirms that the subpycnocline along-channel velocity is also predominantly geostrophic. The BPE density variations below the halocline, however, are not determined by *in situ* processes.

The subhalocline diffusive vertical fluxes of heat and salt are an order of magnitude weaker than the horizontal advective fluxes, and hence variations in the modelled BPE density field owe to advection through geostrophic adjustment to external conditions.

4.3. Density evolution in Penas Gulf

The tight relationship between external density fluctuations and exchange in the BPE is illustrated by the fact that isopycnal evolution in the BPE closely matched that in the south east corner of Penas Gulf (Fig. 6g). The Penas Gulf density field did not, however, simply follow the seasonal cycle in heat and salt fluxes, nor that of the open ocean boundary condition. Despite the fact that maximum warming and freshwater discharge occur in summer, the 1026 kg m^{-3} isopycnal remained depressed in the Penas Gulf and BPE until late winter (Fig. 6g). In fact, the depth of the oceanic 1026 kg m^{-3} isopycnal peaks in February, but the buoyancy of near surface waters continues to increase until May, and a significant shoaling only occurs from August onwards. This lag in Penas Gulf buoyancy loss maintains a relatively thick MSAW layer in the BPE during winter (Fig. 6c and d) that is consistent with the observations (Fig. 3c and d). Thus local processes within Penas Gulf that modify the seasonal oceanic density field control the timing of exchange in the BPE. The processes that determine Penas Gulf density, and in particular the lag in buoyancy loss, are discussed below.

In general agreement with the TSG observations, the surface of the modelled Penas Gulf warmed and freshened over summer. Vertical mixing of the warm fresh surface water, aided by the spring/summer increase in wind stress (Fig. 2c), produces an increasingly deep buoyant surface mixed layer in the model (Fig. 6b). While the warming was relatively evenly distributed across Penas Gulf, freshening was more localised. The surface salinity distribution in Penas Gulf for January and July are given in Fig. 8a and b. Upon exiting the BPE through the south east corner of Penas Gulf, the fresh plume divides into northwards and westwards propagating branches. Although river plumes in the southern hemisphere generally propagate towards the left, the majority of the plume initially propagates towards the right and along the eastern shore of Penas Gulf. The northwards and eastwards advection of the plume is driven by the prevailing westerlies, which drive generally eastwards flow across the surface of Penas Gulf (Fig. 8c and d). As a result, during the spring/summer peak in westerly wind stress and river discharge, the plume is largely retained within Penas Gulf, predominantly along its eastern shore. The freshwater eventually exits Penas Gulf towards the south in autumn/winter, where it is entrained into the Cape Horn Current. The eastwards migration of the plume from summer to winter may be appreciated in the change in position of the 30 psu isohaline in Fig. 8a and b.

Meridional transects at the eastern and western edges of Penas Gulf indicate the existence of mean eastwards flow in a shallow surface layer lying above a clockwise circulation that is intensified towards the coast (Fig. 8c and d). At the western edge of Penas Gulf, the eastwards salinity flux, defined as $FS_x(y, z, t) = u(y, z, t)(S(y, z, t) - S_0)$, where u is the eastwards velocity, S the salinity, and S_0 the mean salinity within Penas Gulf, is eastwards at all depths and latitudes (Fig. 8e), as required to balance the freshwater discharge from the BPE. The clockwise boundary current branches from the Cape Horn Current after rounding the Taitao Peninsula, transporting relatively salty ocean water into Penas Gulf at the northern end of the transect. A net eastwards salinity flux also occurs at the southern extent of the transect (Fig. 8g), corresponding to the westwards transport of freshwater entrained into the current within the Gulf, which reaches its maximum in July. Thus the export of freshwater lags the peak in river discharge by 5 months, indicating that the Penas Gulf remains anomalously fresh until early winter.

In the eastern transect the eastwards surface transport of the fresh plume results in a negative eastwards salinity flux at the surface that is balanced by the transport westwards of brackish waters in the subsurface boundary current (Fig. 8f). While the surface eastwards flux was strongest in summer, the westwards subsurface flux peaked in early winter (Fig. 8h), indicating that freshwater continues to be transported eastwards from the mouth of the BPE at the surface and exported below the surface within the clockwise boundary current well after the peak in freshwater forcing. This implies a vertical salt flux and a freshening of the boundary current along the eastern border of Penas Gulf until July. It is this retention of freshwater close to the mouth of the BPE that delays winter isopycnal shoaling in

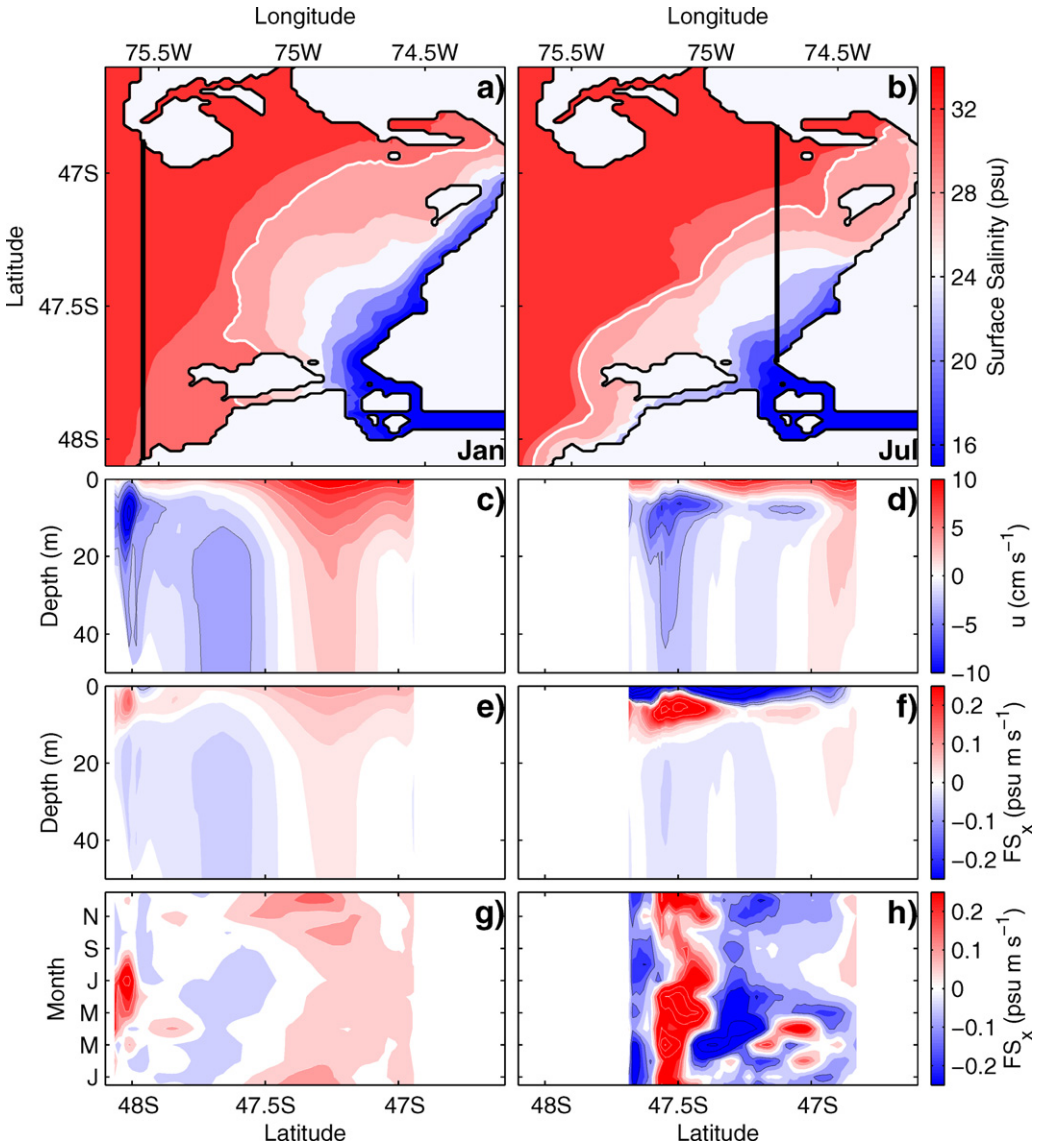


Fig. 8. Mean surface salinity in January (a) and July (b), with the 30 psu isohaline marked by the white contour. Annual mean eastwards velocity (c and d), annual mean eastwards salinity flux (e and f), and monthly mean eastwards salinity flux averaged over the upper 20 m as a function of month, at the western and eastern transects indicated by the black vertical lines in (a) and (b), respectively.

the model. This process may also explain the observed delay in shoaling of the 1026 kg m^{-3} isopycnal within the BPE.

5. Discussion and conclusions

The field campaigns have provided a first record of the seasonal evolution of the water column above sill level along the length of the BPE. Two separate episodes of subsurface warming were observed, and

in each case were inferred to be due to advection of warm water from outside the BPE. The summer warming of EW towards the mouth of the BPE observed in February coincided with a deepening of the 1023 kg m^{-3} isopycnal and the interleaving of warm EW below remnants of cold WW located at the base of the halocline. In the May campaign the MSAW was observed to have warmed and thickened markedly over the autumn. The warming was most apparent at the head of the estuary, resulting in an up-channel temperature gradient in subsurface waters. Relatively warm MSAW at the estuary head and a subsurface temperature gradient were also observed in the winter and spring campaigns, as was observed during the Cimar Fiordo 2 expedition. The properties of the warm subsurface water within the BPE suggest that it was formed during summer within the Penas Gulf. The persistence of warm MSAW at the estuary head over a great part of the year, together with the fact that the thermal structures observed previously in summer and spring are very similar to those observed during this study in the same seasons, implies that the exchange of subhalocline waters between Penas Gulf and the head of the BPE is a seasonally recurrent process. As a result, synoptic processes are implied to be of secondary importance for exchange of intermediary waters at the head of the BPE. Notwithstanding the fact that the exchange is seasonally phase locked, it is nonetheless possible that synoptic processes provide the trigger for the commencement of exchange events.

The possibility for seasonal forcing alone to produce subsurface heating at the head of the BPE was supported by a series of numerical simulations of the circulation in the BPE, Penas Gulf and adjacent ocean. Forcing with the seasonal cycles of run-off and surface fluxes of momentum, heat and salt was sufficient for the model to qualitatively reproduce key features of the observed BPE structure, in particular the evolution of the MSAW layer, including the timing and extent of heating at the head of the estuary. Therefore, while significant synoptic-scale forcing is likely to occur in the real system, it does not appear to play a major role in the evolution of thermal structure at the head of the BPE. Possible effects of subseasonal variability in the lower reaches of the BPE are discussed below.

In the model, heating of MSAW was shown to occur through advection of relatively warm water from Penas Gulf following geostrophic adjustment of the BPE density field to the spring/summer buoyancy increase in the surface oceanic mixed layer. The vertical mixing of relatively buoyant waters is inhibited within the BPE due to the permanent strong pycnocline, and thus the subhalocline density field in the BPE is more tightly coupled to external heat and salt fluxes than to those occurring locally. The observed delay in the shoaling of the base of the MSAW layer relative to the annual cycles of heat flux and river run-off was reproduced in the model, where it was related to the delayed export of relatively buoyant waters from the south eastern corner of the Penas Gulf.

The up-channel temperature gradient implies that the process driving subsurface cooling decreases with distance from the estuary head. While identification of the processes involved is beyond the scope of the present study, a number of candidates may be proposed. The density gradient at the base of the EW layer decreases with distance from the river mouth, such that vertical mixing, and hence winter heat loss to the atmosphere, would be expected to be most strongly suppressed at the head of the channel. As tidal velocities in channels tend to decrease with distance from the channel mouth, tidally induced mixing may be expected to be weakest towards the channel head. Clearly geographical constrictions will tend to create higher tidal velocities and hence greater mixing. In the BPE such features as the Romulo and Remo islands and the Orompello pass are located approximately midway along the length, and do tend to delimit the extent of the channel head warm pool. Finally, although flushing at the estuary head is inferred to be dominantly seasonal, it is possible that synoptic fluctuations in the Penas Gulf density field may drive significant horizontal exchange spatially limited to the mouth of the BPE. The first baroclinic mode will communicate external density changes to the estuary head within a number of days, but it is the rate at which Penas Gulf water intrudes to the BPE that provides the limit upon the axial extent of flushing. For an inflow velocity of 3 cm s^{-1} , as inferred from the observations and model, a water parcel would require ≈ 40 days to transit from Penas Gulf to the mouth of the Pascua river. As a result, external density variability on synoptic scales may flush the mouth of the BPE without affecting the head of the estuary. While each mechanism is plausible, it is anticipated that presently underway and planned observational campaigns will allow their relative importance to be investigated. The fact that the autumn/winter cooling in the lower reaches of the BPE was not reproduced in the model may be due to the absence these various factors.

Seasonal renewal of deep waters in fjords is relatively common (Barnes and Collias, 1958; Gade and Edwards, 1980), and for deep silled fjords the exchange often occurs in summer. In fact, uplift and differential export of the resident deep water following complete renewal events can produce isolated extrema in tracers located at sill level in the upper reaches of the fjord (Gade and Edwards, 1980). The ventilation of intermediate waters, however, commonly has its origin in synoptic off-shore density variability (Stigebrandt, 1990). While the responsible pycnocline fluctuations are typically of mechanical or dynamical origin, in the BPE the seasonal cycle of the off-shore density field, driven solely by the seasonal cycles of heat and salt fluxes over the shelf and adjacent ocean, appears to control flushing above sill level at the estuary head. As discussed above, the persistence of the thermal structure in the upper reaches of the BPE may be in part a function of its length. The presence of the Penas Gulf, however, may also play a role, by buffering the BPE from variability in the adjacent Cape Horn Current and open ocean. For example, while the strength of the Cape Horn Current in the model was greatest in winter, due to the maximum in on-shore Ekman flow, the circulation within Penas Gulf varied weakly through the year. It is not uncommon for the local density field within bays to be insulated from conditions off-shore (e.g. Valle-Levinson and Moraga-Opazo, 2006). Thus it may be that, despite the strong and highly variable wind conditions of the region, the amplitude and duration of the resulting pycnocline fluctuations in Penas Gulf are insufficient to produce flushing that extends beyond the estuary mouth. Given that the Chilean fjords commonly empty to semi-enclosed inland seas or channels, this may explain the recurrence of similar subsurface temperature maxima in various of the internal channels and fjords to the south of the BPE.

Acknowledgements

The assistance in the field work of Paola Ramírez, Jorge Aguila, Maria Vargas and the crew of the *Santa Fe* is gratefully acknowledged. This work was funded by Chilean government FONDECYT project 11060077 and by the assistance of Flanders International and the Flanders Marine Institute to the FOCA project. The manuscript has been greatly improved thanks to the comments of a number of anonymous reviewers.

References

- Aiken, C.M., Petersen, W., Schroeder, F., Gehrung, M., von Holle, P.A.R., 2011. Ship-of-opportunity monitoring of the Chilean fjords using the pocket FerryBox. *J. Atmos. Ocean. Technol.* 28, 1338–1350, <http://dx.doi.org/10.1175/JTECH-D-10-05022.1>.
- Arneborg, L., 2004. Turnover times for the water above sill level in Gullmar fjord. *Cont. Shelf Res.* 24, 443–460.
- Aure, J., Molvær, J., Stigebrandt, A., 1996. Observations of inshore water exchange forced by a fluctuating offshore density field. *Mar. Pollut. Bull.* 33, 112–119.
- Barnes, C.A., Collias, E.E., 1958. Some considerations of oxygen utilization rates in Puget Sound. *J. Mar. Res.* 17, 68–80.
- Cottier, F.R., Nilsen, F., Inall, M.E., Gerland, S., Tverberg, V., Svendsen, H., 2007. Wintertime warming of an Arctic shelf in response to large-scale atmospheric circulation. *Geophys. Res. Lett.*, 34.
- Farmer, D.M., Freeland, H.J., 1983. The physical oceanography of fjords. *Prog. Oceanogr.* 12, 147–220.
- Fer, I., 2009. Weak vertical diffusion allows maintenance of cold halocline in the central arctic. *Atmos. Ocean. Sci. Lett.* 2 (3), 148–152.
- Fuenzalida, H., Aceituno, P., Falvey, M., Garreaud, R., Rojas, M., Sanchez, R., 2007. Study on climate variability for Chile during the 21st century. Conama tech. rep., Geophysics Department, University of Chile. Available from: <http://www.dgf.uchile.cl/PRECIS>.
- Gade, H.G., Edwards, A., 1980. Deep water renewal in fjords. In: Freeland, H.J., Farmer, D.M., Levings, C. (Eds.), *Fjord Oceanography*. Plenum, London, pp. 453–489.
- Guzmán, D., Silva, N., 2002. Caracterización física y química y masas de agua en los canales australes de Chile entre Boca de Guafo y Golfo Elefantes (Crucero Cimar Fiordo 4). *Cienc. Tecnol. Mar.* 25 (2), 45–76.
- Hetland, R.D., 2005. Relating river plume structure to vertical mixing. *J. Phys. Oceanogr.* 35, 1667–1688.
- Janzen, C., Simpson, J.H., Inall, M.E., Cottier, F.R., 2005. Cross-sill exchange and frontal flows over the sill of a broad fjord. *Cont. Shelf Res.* 25, 1805–1824.
- Klinck, J.M., O'Brien, J.J., Svendsen, H., 1981. A simple model of fjord and coastal circulation interaction. *J. Phys. Oceanogr.* 11, 1612–1626.
- Large, W.G., McWilliams, J., Doney, S., 1994. Oceanic vertical mixing: a review and a model with a nonlocal boundary layer parameterization. *Rev. Geophys.* 32, 363–403.
- MacCready, P., Geyer, W.R., 2001. Estuarine salt flux through an isohaline surface. *J. Geophys. Res.* 106, 11629–11637.
- Marchesiello, P., McWilliams, J., Shchepetkin, A., 2001. Open boundary conditions for long-term integration of regional ocean models. *Ocean Modell.* 3, 1–20.
- Mellor, G.L., Ezer, T., Oey, L.-Y., 1994. The pressure gradient conundrum of sigma coordinate ocean models. *J. Atmos. Ocean. Technol.* 11, 1126–1134.

- Padman, L., Dillon, T.M., 1987. Vertical heat fluxes through the Beaufort sea thermohaline staircase. *J. Geophys. Res.* 92, 10779–10806.
- Pickard, G., 1971. Some physical oceanographic features of inlets of Chile. *J. Fish. Bd. Canada* 28, 1077–1106.
- Pickard, G.L., Stanton, B.R., 1980. Pacific fjords—a review of their water characteristics. In: Freeland, H.J., Farmer, D.M., Levings, C. (Eds.), *Fjord Oceanography*. Plenum, London, pp. 1–52.
- Rojas, R., Calvete, C., Guerrero, Y., Silva, N., 2002. Reporte de datos de crucero oceanográfico CIMAR 2 FIRDOS [CD-ROM].
- Shchepetkin, A.F., McWilliams, J.C., 2005. The regional ocean modelling system: a split-explicit, free-surface, topography following coordinates ocean model. *Ocean Modell.* 9, 347–404.
- Sievers, H., Calvete, C., Silva, N., 2001. Distribución de características físicas, masas de agua y circulación general para algunos canales australes entre el golfo de Penas y el estrecho de Magallanes (Crucero Cimar-Fiordo 2), Chile. *Ciencia y Tecnología del Mar*.
- Sievers, H., Prado, R., 1994. Contraste de las características oceanográficas del seno Aysén, Chile, entre invierno y verano (lat. 45° 20' S). *Rev. Biol. Mar. Valparaíso* 29 (2), 167–209.
- Silva, N., Calvete, C., 2002. Características oceanográficas físicas y químicas de canales australes chilenos entre el Golfo de Penas y el Estrecho de Magallanes (crucero Cimar-Fiordo 2). *Cienc. Tecnol. Mar.* 25, 23–88.
- Silva, N., Calvete, C., Sievers, H., 1998. Masas de agua y circulación general para algunos canales australes entre Puerto Montt y Laguna San Rafael, Chile. *Cienc. Tecnol. Mar.* 21, 17–48.
- Silva, N., Guzmán, D., 2006. Condiciones oceanográficas físicas y químicas, entre la boca del Guafo y fiordo Aysén (Crucero CIMAR 7 Firdos). *Cienc. Tecnol. Mar.* 29 (1), 25–44.
- Silva, N., Neshyba, S., 1977. Corrientes superficiales frente a la costa austral de Chile. *Cienc. Tecnol. Mar.* 3, 37–42.
- Silva, N., Sievers, H., Prado, R., 1995. Descripción oceanográfica de los canales australes de Chile. Zona Puerto Montt – Laguna San Rafael (41° 20' S). *Rev. Biol. Mar.* 30 (2), 207–254.
- Song, Y., Haidvogel, D.B., 1994. A semi-implicit ocean circulation model using a generalized topography-following coordinate system. *J. Comp. Phys.* 115 (1), 228–244.
- Stigebrandt, A., 1990. On the response of the horizontal mean vertical density distribution in a fjord to low-frequency density fluctuations in the coastal water. *Tellus* 42A, 605–614.
- Svendsen, H., 1980. Exchange processes above sill level between fjords and coastal water. In: Freeland, H.J., Farmer, D.M., Levings, C. (Eds.), *Fjord Oceanography*. Plenum, London, pp. 355–362.
- U.S. Department of Commerce, N.O., Atmospheric Administration, N.G.D.C., 2006. 2-Minute gridded global relief data, ETOPO2v2.
- Valle-Levinson, A., Moraga-Opazo, J., 2006. Observations of bipolar residual circulation in two equatorward-facing semiarid bays. *Cont. Shelf Res.* 26, 179–193.
- Warner, J.C., Geyer, W.R., Lerczak, J.A., 2005. Numerical modeling of an estuary: a comprehensive skill assessment. *J. Geophys. Res.* 110.
- Wunsch, C., Heimbach, P., 2007. Practical global oceanic state estimation. *Physica D* 2301–2, 197–208.